Three Distinct Torsion Profiles of Electronic Transmission through Linear Carbon Wires

Marc H. Garner[†], William Bro-Jørgensen, Gemma C. Solomon*

Nano-Science Center and Department of Chemistry, University of Copenhagen,

Universitetsparken 5, DK-2100 Copenhagen Ø, Denmark.

ABSTRACT. The one-dimensional carbon allotrope carbyne, a linear chain of *sp*-hybridized carbon atoms, is predicted to exist in a polyynic and a cumulenic structure. While molecular forms of carbyne have been extensively characterized, the structural nature is hard to determine for many linear carbon wires that are made in-situ during pulling experiments. Here, we show that cumulenes and polyynes have distinctively different low-bias conductance profiles under axial torsion. We analyze the change of the electronic structure, Landauer transmission, and ballistic current density of the three types of closed-shell molecular carbynes as a function of the torsion angle. Both polyynic, odd-carbon cumulenic, and even-carbon cumulenic carbon wires exhibit helical frontier molecular orbitals when the end-groups are not in a co-planar configuration. This helical conjugation effect gives rise to strong ring current patterns around the linear wires. Only the transmission of even-carbon polyynic wires follows the well-known cosine-squared law with axial torsion that is also seen in biphenyl-type systems. Notably, the transmission of even-carbon cumulenic carbon wires rises with axial torsion from co-planar towards perpendicular orientation of the end-groups. The three distinct transmission profiles of polyynes, odd-carbon cumulenes,

and even-carbon cumulenes may allow for experimental identification of the structural nature of linear carbon wires. Their different electron transport properties under axial torsion furthermore underline that, in the molecular limit of carbyne, three different subclasses of linear carbon wires exist.

INTRODUCTION

The elusive one-dimensional carbon allotrope carbyne attracts much interest due to a number of proposed properties that may be desirable for materials and molecular electronics.[1-2] Depicted in Figure 1a, carbyne is a linear chain of *sp*-hybridized carbon atoms and exists in two configurations: The polyynic type with bond-length alternation, and the cumulenic type with equal bond lengths. The specific properties depend on the type of carbyne; for example, polyynic carbyne is predicted to be a semiconductor while cumulenic carbyne is metallic.[3-8] However, as inferred by the ball-and-stick models in Figure 1, when bond lengths cannot be determined it is fundamentally difficult to assess the polyynic or cumulenic nature of carbon wires.

Molecular carbon wires have attracted broad interest as model systems for carbyne, and both polyynes and cumulenes of substantial length have been reported.[9-13] These molecular wires, exemplified in Figure 1b, have the advantage that their structure and properties can be analyzed with the spectroscopic tools of modern chemistry.[1, 12-13] However, their properties may not fully reflect that of extended structures. Illustrated in Figure 1c, an extended carbyne system can be formed by letting the molecule bridge a nanoscale gap between two metal electrodes. The electron transport properties of several short molecular carbynes have been examined experimentally in single-molecule junctions for both polyynic and cumulenic molecular wires.[14-20] In single-molecule junctions the chemical structure of the isolated molecule is typically retained, and therefore the

polyynic or cumulenic configuration of the molecular wire can be controlled by chemical design. A third type of carbyne-like system is illustrated in Figure 1d. Linear carbon wires have been made experimentally by pulling from carbon-based electrodes or inside carbon nanotubes.[21-27] However, the properties of these out-of-equilibrium carbon wires produced in-situ during pulling experiments are somewhat elusive, and the polyynic or cumulenic nature of the wires is not straightforward to identify.[2] Given these wires are still within the molecular limit of carbyne (lengths of tens or few hundreds of atoms), we suggest that axial torsion of extended carbon wires is a reliable way to distinguish the two (or three) types of carbyne structures from each other.
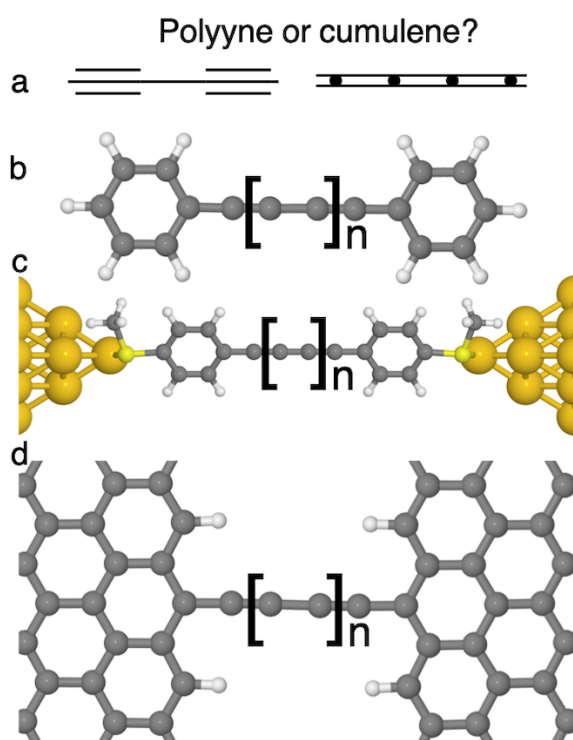

Figure 1. a) Polyynic and cumulenic Kekulé structures of carbyne. b) Ball-and-stick model of a molecular carbyne wire. c) Ball-and-stick model of a functionalized molecular carbyne bridging two metal electrodes in a single-molecule junction. d) Ball-and-stick model of an extended carbon structure with a carbyne unit bridging two carbon-based electrodes, e.g., graphene.

AXIAL TORSION OF MOLECULES. Axial torsion is a fundamental degree of freedom in many molecules and has been studied extensively in the context of molecular electronics. The low-bias single-molecule conductance of a functionalized biphenyl molecule follows a cosine-squared law of the dihedral angle between the two benzene rings.[28-32] This dependence follows directly from the overlap integral of two p-orbitals on adjacent atoms, which has a cosine dependence on the dihedral angle between the two orbitals as sketched in Figure 2a. In any molecule where two otherwise separate π-systems couple directly through a single π-interaction, we expect to see the cosine-squared dependence in the off-resonant electronic transmission as a function of the torsion dihedral angle. Biphenyl is perhaps the most studied example of such a situation.[33-35]
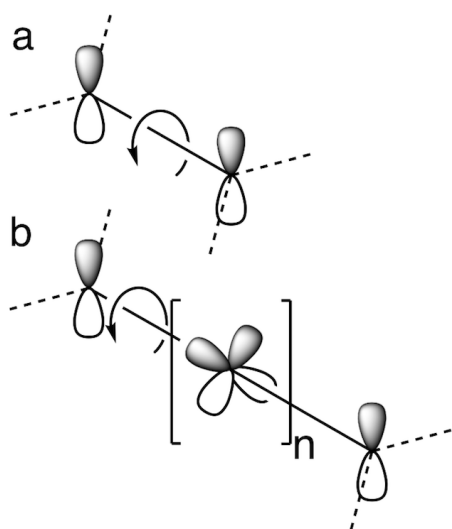

Figure 2. Two simplified cases of coupling between two p-orbitals during axial torsion. a) direct coupling through a single π-bond, e.g. the case of biphenyl. b) Coupling mediated by a coarctate orbital-system, e.g., a polyynic or cumulenic carbon bridge of arbitrary length.

Now we extend the first case into a system where two π-systems couple through a linear *sp*-hybridized carbon bridge. As illustrated in Figure 2b, a fundamental difference is apparent from the system shown in Figure 2a. The two terminal π-systems can couple through what may be

considered as two orthogonal π-systems on the linear carbon bridge. However, the orbital system on the linear carbon bridge can be oriented in any way, and can be depicted as a continuously overlapping cyclic p-orbital basis as specifically illustrated in Figure 2b.[36-38] In this "coarctate" orbital basis there is an unbroken overlap through the carbon wire that connects the two terminal π-systems even when they are rotated 90° relative to each other. This coarctate orbital topology appears in linear carbon molecules of both the polyynic and cumulenic type, and we recently described this in detail.[39]

In the molecular orbital picture, the possibility of electronic coupling between perpendicular end-groups of an *sp*-hybridized carbon wire manifests itself in the form of helical molecular orbitals that span the entire length of the linear carbon bridge.[39-47] Such helical π-orbitals appear in linear carbon wires upon a suitable reduction of symmetry due to substituents or axial torsion. Consequently, a molecule can be single-handed chiral while orbitals of both helicities appear; this has serendipitously been shown for a number of linear molecular systems.[48-54] Despite having perpendicular end-groups in their ground-state structure, odd-carbon cumulenes with pyramidalized single-faced π-donor substituents can achieve high electronic transmission similar to that of even-carbon cumulenes and polyynes.[45-46, 55] Furthermore, helical π-orbitals can give rise to ring currents around the linear wire where the circular direction of the current is controlled by the helicity of the frontier orbitals. The understanding of the relation between helical molecular orbitals, electronic transmission, and ring currents in linear systems is still in its infancy.[45, 56] Motivated by the insight local pictures of ballistic current provide for aromatic hydrocarbons,[57-62] we will address this issue further in this study.

MOLECULAR CARBYNES. In the molecular limit of carbyne, there are not only two, but three types of stable closed-shell molecules. Closed-shell polyynes only exist as even-carbon

systems with alternating single and triple bonds. Like in biphenyl systems, there is almost free rotation for the end-groups of polyynic wires as exemplified by the torsion energy profile in Figure 3 and Figure S1. Cumulenes exist both as even- and odd-carbon closed-shell systems; for the remainder of the manuscript we will adhere to the chemical nomenclature and refer to them as even-n and odd-n [n]cumulenes, where n is the number of cumulenic double bonds (the number of carbon atoms is thus n+1).[13] Odd-n cumulenes have co-planar end-groups in their ground-state structure with considerable torsion barriers.[20, 63-67] As shown in Figure 3, even-n cumulenes have similar torsion barriers, however, the end-groups are perpendicular in the ground-state structure where the molecules have a closed-shell electronic structure. This remarkable structural difference between the odd-n and even-n cumulenes means that they are almost as different from each other as they are to polyynes. Although the electronic and transport properties of closed-shell cumulenes and polyynes have been described extensively,[6-8, 43, 55, 68-71] the structural differences between odd-n and even-n cumulenes has been overlooked in the charge transport literature and has been interpreted as an odd-even effect.[3-5, 72-84] We will argue such an interpretation is not always meaningful in the molecular limit of carbyne, as we demonstrate in this work that the charge transport properties of the two cumulene types are fundamentally different.
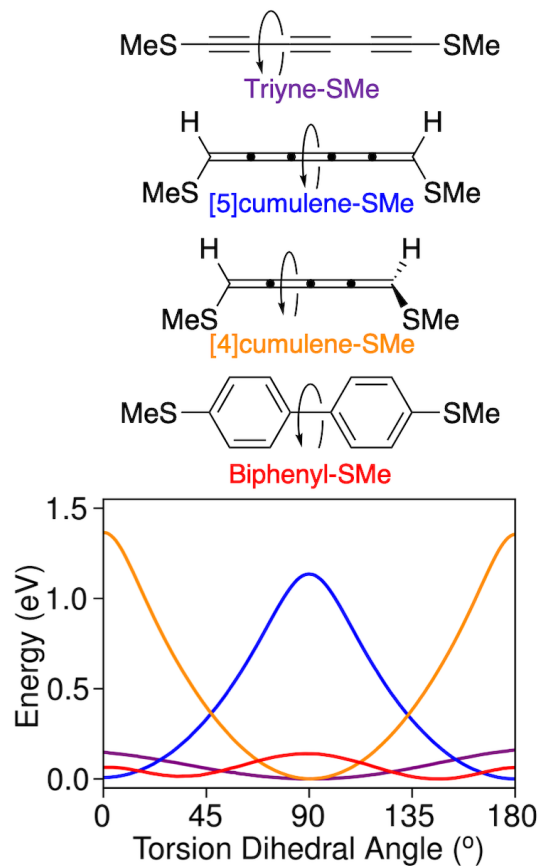
Figure 3. Axial torsion energy profile of three types of thiomethyl-functionalized linear carbon wires and the equivalent biphenyl. The computational details are described in the methods section and in SI part A.

In this article we revisit axial torsion of polyynic and cumulenic carbon wires and analyze the electronic structure, Landauer transmission, and ballistic current density of thiomethyl-functionalized **triyne-SMe**, **[5]cumulene-SMe**, and **[4]cumulene-SMe** illustrated in Figure 3, as well as the equivalent **biphenyl-SMe**. We apply our recently developed s-band electrode transmission code,[85] which allow for realistic coupling into the contact groups with only a minimal perturbation of the electronic structure of the molecule thereby allowing us to draw general conclusions.

The article is structured as follows. In the following three sections we present the results for each of the three molecular types of carbyne: polyynic, odd-*n* cumulenic, and even-*n* cumulenic. After a brief introduction of each type of wire, each section covers the change of the electronic structure and electron transport properties during axial torsion. We identify three distinct torsion profiles for the low-bias single-molecule conductance, supporting the view molecular carbynes must be considered as three distinct classes of closed-shell carbon wires: polyyne, odd-*n* cumulene, and even-*n* cumulene. Before concluding on the findings, we provide a discussion of the results, the theoretical approach, and its possible limitations.

METHODS

In this work we explored the electronic structures and electron transport properties of linear carbon molecules under axial torsion. The molecular structures were preliminarily optimized to the *verytight* criteria using DFT with the Perdew-Burke-Ernzerhof (PBE) functional and 6-311G(d,p) basis set as implemented in Gaussian09.[86-87] The dihedral angles were manipulated directly on the optimized structure of each molecule without further optimization. Specifically, these were the Me-S—S-Me dihedral angle for **triyne-SMe** (long line indicating that the two atoms are not nearest neighbors), the S-C—C-S dihedral angles for **[4]cumulene-SMe** and **[5]cumulene-SMe**, and one of the C-C-C-C dihedral angles (connecting the two rings) for **biphenyl-SMe**.

All electronic structure calculations presented in the manuscript were carried out using DFT as implemented in Atomic Simulation Environment (ASE) and GPAW.[88-89] We used the PBE functional with double-ζ plus polarization (DZP) basis set for all atoms.[90] This level of theory was chosen in order to carry out the transport calculations. Based on the torsion energy profiles (Figure 3) which we have also calculated at the M06-2X(D3) level of theory as implemented in Gaussian09

and CASSCF as implemented in Dalton (Figure S1),[87, 91-93] we expect results to be qualitative similar at higher levels of theory. All molecular structures, orbitals, and current density plots were made using Jmol.[94] Molecular orbitals were plotted using the default isosurface value of 0.02.

Electron transport calculations were carried out using the non-equilibrium Green's functions (NEGF) approach in combination with DFT as implemented in ASE and GPAW,[88-89] or with a Hückel model where noted. The retarded and advanced Green's functions, $G^{r/a}(E)$, are calculated from the Hamiltonian and overlap matrix of the molecular region, H_M and S_M, and the self-energies of the left and right electrodes, $\Sigma_{L/R}^{r/a}(E)$,

$$G^{r/a}(E) = \left[E \cdot S_M - H_M - \Sigma_L^{r/a}(E) - \Sigma_R^{r/a}(E)\right]^{-1}. \qquad (1)$$

The Landauer transmission, $T(E)$, is then calculated using the coupling matrices of the left and right electrodes, $\Gamma_{L/R}$,

$$T(E) = \text{tr}[\Gamma_L(E)G^r(E)\Gamma_R(E)G^a(E)]. \qquad (2)$$

Except where otherwise noted, electron transport and current density calculations presented in the manuscript are modelled using single-molecule junctions with s-band electrodes. These junctions were formed using two dihydrogen molecules placed with an S-H distance of 1.75 Å, a C-S-H bond angle X 110°, and C-C-S-H dihedral angle of 120° (for **triyne-SMe** this is defined by the methyl group), thus forming the extended molecular region used in equation 1. The s-band electrodes were formed using the wide-band approximation with nonzero matrix elements of $\Gamma_{L/R}$ set to $\gamma = 1.0$ eV. This approach gives a qualitatively similar transmission to using periodic Au-electrodes, and allows us to calculate the ballistic current density.[56, 85] Both transmission and current density calculations were carried out using DFT with the PBE functional and DZP basis set for all atoms except hydrogen where a SZ basis was used. A Fermi temperature is applied to ensure convergence for systems with vanishing HOMO-LUMO gap, which corresponds to a width

of 0.1 in the Fermi function. We carried out these calculations using our homemade transport and current density code which is compatible with GPAW and ASE,[88-89] and freely available at https://github.com/marchgarner/Current_Density.git; a brief description of the approach follows here.

At zero-temperature and absent of an external magnetic field, the low-bias current density, $\mathbf{j(r)}$, can be calculated using the NEGF formalism as described by equation 3.

$$\mathbf{j(r)} = \frac{ie^2\hbar}{4m\pi}\sum_{i,j\in C}\int_{-\infty}^{\infty} dE \ G_{ij}^n \left[\psi_i(\boldsymbol{r})\nabla\psi_j(\boldsymbol{r}) - \psi_j(\boldsymbol{r})\nabla\psi_i(\boldsymbol{r})\right] \qquad (3)$$

Here ψ are basis functions and C are the indices of functions within the extended molecular region which we sum over.[95-96] G^n is the non-equilibrium part of the lesser Green's function and δV is a small symmetric bias difference between the electrodes, which we set to $\delta V=1 \ mV$.

$$G^n = iG^r\Gamma_L G^a \delta V \qquad (4)$$

Each vector in the $\mathbf{j(r)}$ vector field is plotted as an arrow of same length; the vector-length (the magnitude of the current density at position $\mathbf{r}$) is the radius of the arrow and is scaled relative to the largest arrow in the same figure. Vectors smaller than 5% of the largest z-component are not included for clarity, z being the transport direction. We calculated the current density in a cylindrical coordinate system, which allow us to color the arrows by the relative cylindrical vector-component $\frac{v_\theta}{|\vec{v}|}$. The conversion from cartesian to cylindrical coordinates is trivial, and is included for reference in SI part H. Finally, as we and other have recently noted,[45, 56, 97-100] ballistic current density calculations can have serious issues with current conservation over the molecule due to using a finite local basis set and approximated core-potentials; we provide some examples of this problem in SI part G.

As described in the Discussion section, we also carried out transport calculations using two alternative calculation setups. For the most simplistic approach to coherent electron transport, we

produced Hückel models for each molecule, which is described in detail in SI part F. For more realistic modelling of Au-molecule-Au junctions, we carry out the calculations using DFT as implemented in ASE and GPAW with the PBE functional and DZP basis set for all atoms. [86, 88-90] The junction structure is formed by placing the molecular structure between two 4-atom Au pyramids on 4×4 Au(111) surfaces with periodic boundary conditions in the plane of the surfaces. From this junction structure the Landauer transmission is calculated using equation 2 with a k-point sampling over a $4 \times 4 \times 1$ Monkhorst–Pack mesh in the first Brillouin zone.

POLYYNIC CARBON WIRES

Polyynes are linear chains of *sp*-hybridized carbon where the bonds formally alternate between single and triple bonds, and accordingly there is a low torsion barrier in such molecules as exemplified in Figure 2. The strong bond-length alternation opens the HOMO-LUMO gap and contributes to making polyynes more stable than cumulenes of equivalent length. With reasonable kinetic and thermodynamic stability, the single-molecule conductance of polyynes has been measured experimentally in single-molecule junctions as long as a hexyne (a 14 atom long linear carbon molecule).[14-18]

ELECTRONIC STRUCTURE. Shown in Figure 4, four frontier molecular orbitals and their eigenvalues are calculated for the **triyne-SMe**. The two π-orbital systems are separated by symmetry when end-groups are co-planar at 0° and 180°, and the π–orbitals take their normal rectilinear shape. The shape of the molecular orbitals immediately changes towards a helical shape when the end-groups are rotated into a non-planar geometry because the symmetry of the molecule is reduced. This is the helicogenic symmetry (C_2 or D_2) we have previously identified.[39] Polyynes

with non-planar end-groups will exhibit some degree of helical molecular orbitals due their helicogenic symmetry, and a number of such molecules have already been synthesized.[101-105]

Starting from 0° in Figure 4 we can trace the gradual evolution of the molecular orbitals. The two orbital pairs (HOMO–1 and HOMO, LUMO and LUMO+1) are each separated in energy by ~1 eV. As the molecule is twisted towards 90° the energy separation between in each orbital pair decreases and the HOMO-LUMO gap becomes slightly larger. At 30° the helicity of each molecular orbital is visually clear. The HOMO (orange in Figure 4) is a minus helix and as we apply a clockwise torsion of the molecule this helix is being unwound, and consequently its eigenvalue decreases. The HOMO–1 (red in Figure 4) is a plus helix and consequently it is being overwound with the torsion of the molecule and its eigenvalue increases. As the eigenvalues change in opposite directions the HOMO–1 and HOMO "switch place" at 90°, as do the LUMO and LUMO+1. From 90° to 180° the energy splitting of the two orbital pairs is recovered and the HOMO-LUMO equivalently becomes smaller. Finally, at 180° the original π-orbitals are recovered as the HOMO (orange) has been changed into an orbital equivalent to the original HOMO–1 (red) and vice-versa. By visual inspection it is clear from Figure 4 that the molecular orbitals appear more helical close to 90°; we are working towards quantifying this orbital helicity in future work.
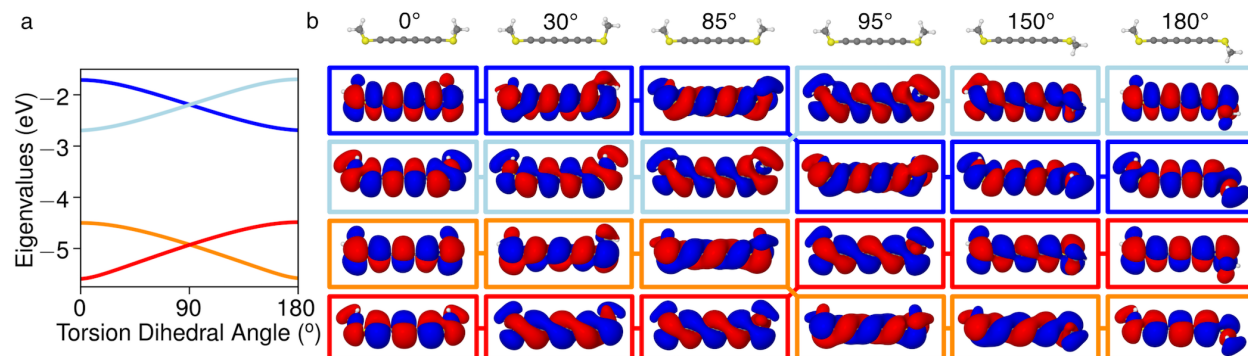
Figure 4. Change of the frontier molecular orbitals of **triyne-SMe** under axial torsion. a) Eigenvalues of the frontier molecular orbitals plotted as a function of dihedral angle. b) Iso-plot of the four frontier molecular orbitals at dihedrals angles of 0°, 30°, 85°, 95°, 150°, and 180°, the molecular structures are shown at the top, followed by the LUMO+1, LUMO, HOMO, and HOMO–1 at the bottom.

ELECTRON TRANSPORT. Shown in Figure 5, the current density and electronic transmission is calculated for **triyne-SMe** under axial torsion. With co-planar end-groups the current follows a largely linear path (arrows are almost white due to the small θ-component, see also Figure S17 and S20) as we may expect for a linear π-system. As torsion is applied ring currents become increasingly clear around the wire. As can be seen in Figure 5a, at 0° and 180° torsion weak ring currents are centered at the carbon atoms. At 85° and 95° torsion strong ring currents are centered around the two formal single-bonds of the carbon wire, see also Figure S18 and S19. The direction of the circular component of the current reverses at 90°, which can be observed by the change of the color of the arrows from blue to red. It is at 90° that the helicity of the HOMO and LUMO changes because of the torsion (see Figure 4), underlining the correlation between the helicities in the electronic structure and the direction of the ballistic ring currents.

At 0° and 180° the transmission is high, as we may expect from having a fully π-conjugated transport path through the molecule. Shown in Figure 5b and 5c, the transmission is effectively suppressed by axial torsion towards 90°, and follows a $\cos^2$ dependence like **biphenyl-SMe**. At 90° the transmission does not completely go to zero, which is most likely due to transmission mediated by the σ-system. This large transmission difference by torsional control of the end-groups has previously been suggested as a means to achieve electronic functionality in polyyne-based molecular devices.[106-109] The suppression happens as the HOMO and HOMO–1 (LUMO and

13

LUMO+1) become degenerate at ~90° (see Figure 4), and consequently the transmission through the helical π-systems is fully suppressed. Rather than due to two orthogonal π-systems, we consider the low transmission at 90° as a consequence of destructive quantum interference effect due to near-degeneracy of two helical orbitals with opposite symmetries. We will return to this with clear examples in the discussion section. The reversal of the ring currents at 90° is also intimately linked to this interference effect.[45,57,61] The full transmission plots at 95°, 150° and 180° are almost identical to those at 85°, 30°, and 0° and are shown in Figure S4.
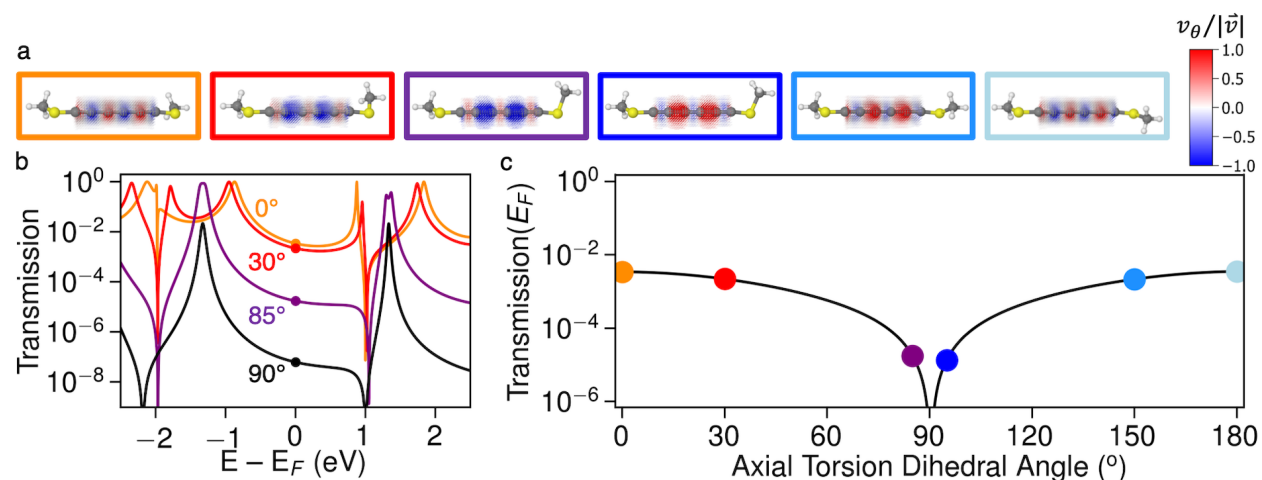

Figure 5. Current density and transmission of **triyne-SMe** under axial torsion. a) Current density calculated at the Fermi energy colored by the normalized θ vector component at dihedral angles (from left to right) 0°, 30°, 85°, 95°, 150°, and 180°. The current density vector field is plotted as arrows that are normalized in each plot; each arrow is colored by its circular vector component (v_θ) normalized relative to its total vector length. High resolution images are included in SI part H, and scripts for generating 3D rotatable models are available online. b) Transmission plotted semilogarithmically against energy at select dihedral angles. c) Transmission at the fermi energy plotted against the torsion dihedral angle.

Cumulenes are linear chains of *sp*-hybridized carbon with consecutive formal double-bonds and consequently there is almost no bond-length alternation.[13] Like polyynes, odd-*n* cumulenes have an even number of carbon atoms in the linear chain. Consequently, odd-*n* cumulenes have co-planar end-groups in their closed-shell ground-state structure (see Figure 3). Although less stable than polyynes, [9]cumulenes have been characterized, and functionalized [3]- and [5]cumulenes have been measured in single-molecule junction experiments.[13, 19-20] The single-molecule conductance of odd-*n* cumulenes is expected to be higher than that of equivalent polyynes due to the smaller bond-length alternation, which narrows the HOMO-LUMO gap.[55]

ELECTRONIC STRUCTURE. The four frontier molecular orbitals and their eigenvalues are calculated for the **[5]cumulene-SMe** in Figure 6. At 0° and 180°, the two π orbital systems are separated by symmetry because the end-groups are co-planar, and the π orbitals take their usual rectilinear shape. The two π-systems are non-degenerate as the in-plane π-system spans only four carbon atoms, while the out-of-plane π-system spans all six carbon atoms. As with the polyynes, the shape of the molecular orbitals immediately changes towards a helical shape when the end-groups are rotated into a non-planar geometry because the symmetry of the molecule is reduced and a helicogenic symmetry is achieved.[39, 43]

Starting from 0° in Figure 6, we can trace the gradual evolution of the molecular orbitals. Starting out at 0°, each of the two orbital pairs (HOMO–1 and HOMO, LUMO and LUMO+1) are close in energy. Under torsion the HOMO-LUMO gap rapidly narrows and at 90° the HOMO and LUMO become degenerate and cross. The frontier molecular orbitals of the non-planar molecules have clear helicity, which changes at 90°. Shown in Figure 6b, the HOMO and LUMO (light-blue and orange in Figure 6) switch place at 90°. Likewise, the HOMO–1 interchange with the HOMO–2,

and the LUMO+1 with the LUMO+2. From the perspective of orbital helicity, the LUMO eigenvalue is lowered by the torsion as the orbital-helix is being unwound; the HOMO eigenvalue rises as the orbital-helix is being overwound by the axial torsion. The molecule formally becomes a diradical at 90° and we note that a multi-reference computational approach must be used to fully assess the transport and electronic properties of this transition state, rather than the singlet ground-state approach we apply here;[110] see SI part A for a brief comparison of methods.
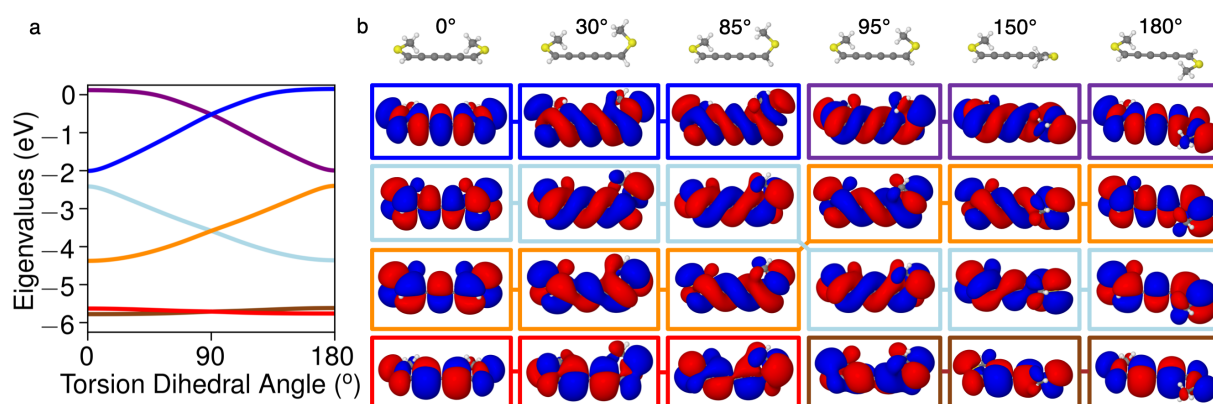

Figure 6. Change of the frontier molecular orbitals of **[5]cumulene-SMe** under axial torsion. a) Eigenvalues of the frontier molecular orbitals (from HOMO–2 to LUMO+2) plotted as a function of dihedral angle. b) Iso-plot of the four frontier molecular orbitals at dihedrals angles of 0°, 30°, 85°, 95°, 150°, and 180°, the molecular structures are shown at the top, followed by the LUMO+1, LUMO, HOMO, and HOMO–1 at the bottom.

ELECTRON TRANSPORT. Shown in Figure 7, the ballistic current density and electronic transmission is calculated for **[5]cumulene-SMe** under axial torsion. With co-planar end-groups at 0° and 180° torsion, the current follows a largely linear path through the π-system (current density arrows are almost white due to the small θ vector-component, see also Figure S21 and S24). As in the case of **triyne-SMe** at 0° and 180° torsion (Figure 5), there are weak ring currents

centered at the carbon atoms alternating in direction with every atom. These ring currents become increasingly clear around the wire when axial torsion is applied as seen by the change of color towards stronger blue and red colors (clockwise and counter-clockwise directions). At 85° and 95° torsion, strong ring currents are centered around the bonds of the carbon wire, now alternating in direction with every cumulenic bond. The ring current pattern reverses at 90°, again in correlation with the HOMO and LUMO helicity interchanging (see Figure 6).

The transmission profile of odd-n cumulenes is quite distinct from that of the polyyne. Shown in Figure 7c for **[5]cumulene-SMe**, under axial torsion from the two ground-state structures at 0°/180° the transmission at the Fermi energy rises almost until 90° torsion. Despite that the end-groups are almost perpendicular at 85°/95° torsion the transmission is very high. The increase of transmission with torsion towards 90° is a direct consequence of the decreasing HOMO-LUMO gap and will be accompanied by an increase in the diradical character of the molecule.[55, 111] As the HOMO-LUMO gap vanishes, electron transport under bias will eventually change from off-resonant to resonant tunneling, although only few molecular systems have been reported which achieve resonant transport without a gate-electrode.[112-113]

At 90° there is a steep drop of the transmission because the HOMO and LUMO become near-degenerate. As with the **triyne-SMe** at 90° torsion, the orbital symmetries mean that the transmission is suppressed when frontier molecular orbitals become degenerate due to destructive quantum interference, a point we will describe in more detail in the discussion section. The close relation to destructive quantum interference in aromatic molecules is also evident by the fact that the directions of the ring currents revert at 90° torsion.[57] The full transmission plots at 95°, 150° and 180° are almost identical to those at 85°, 30°, and 0° and are shown in Figure S4.
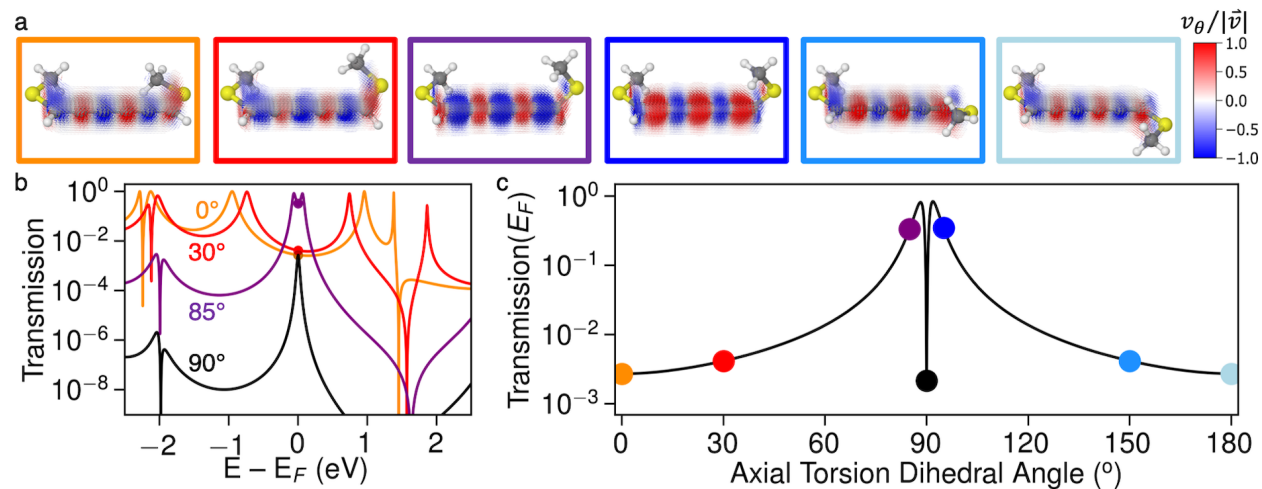
Figure 7. Current density and transmission of **[5]cumulene-SMe** under axial torsion. A) Current density calculated at the Fermi energy colored by the normalized θ vector component at dihedral angles (from left to right) 0°, 30°, 85°, 95°, 150°, and 180°. The current density vector field is plotted as arrows that are normalized in each plot; each arrow is colored by its circular vector component (v_θ) normalized relative to its total vector length. High resolution images are included in SI part H, and scripts for generating 3D rotatable models are available online. b) Transmission plotted semilogarithmically against energy at select dihedral angles. c) Transmission at the fermi energy plotted against the torsion dihedral angle.

EVEN-*n* CUMULENIC CARBON WIRES

Even-*n* cumulenes have many of the same structural traits as the odd-*n* cumulenic systems with almost no bond-length alternation, lower stability than polyynes, and considerable axial torsion barriers (see Figure 3). Unlike the other two types of linear carbon wires, even-*n* cumulenes have an odd number of carbon atoms in the linear chain and achieve closed-shell electronic structure by having perpendicular end-groups. Owing to the orientation of the end-groups, there is not much

electronic communication through the π-systems of the molecule; the single-molecule conductance of a functionalized [2]cumulene (allene) was recently measured to be almost two orders of magnitude lower than that of the equivalent [3]cumulene.[19] However, we recently demonstrated that the electronic transmission through even-n cumulenes can be almost as high as that of the equivalent odd-n systems by splitting the helical frontier molecular orbitals using pyramidalized π-donor substituents. Strategies for manipulating the helical electronic structure of cumulenes using substituents is described in detail elsewhere.[39-40, 45-47]

ELECTRONIC STRUCTURE. The four frontier molecular orbitals and their eigenvalues are calculated for the **[4]cumulene-SMe** in Figure 8. In the ground-state structure at approximately 90°, each of the helical orbital pairs (HOMO-1 and HOMO, LUMO and LUMO+1) are near-degenerate. Depending on the torsion away from 90° the orbital pairs split in each direction and the HOMO-LUMO gap narrows. As in the previous two cases, the molecular orbitals have a clear helical shape when the end-groups are in a non-planar geometry (including that at 90°) because a helicogenic symmetry is achieved.[39, 43]

The orbital helicity of the HOMO and LUMO will vary as different helical orbitals are (de)stabilized depending on the direction of the axial torsion from the ground-state structure at 90°. This is seen in Figure 8, for example by comparing the helicities of the HOMO at 30° and 150°, in the first case a minus helix and in the second case a plus helix. We can trace the gradual evolution of the molecular orbitals from 90° towards 0° in Figure 8. As torsion is applied from 85° to 30°, the HOMO (orange in Figure 8) is destabilized as it is a helix that is being overwound, and the LUMO (light-blue in Figure 8) is stabilized as it is a helix that is being unwound. Thus, the HOMO-LUMO gap narrows and almost vanishes at 0°. At 0° and 180°, the two π orbital

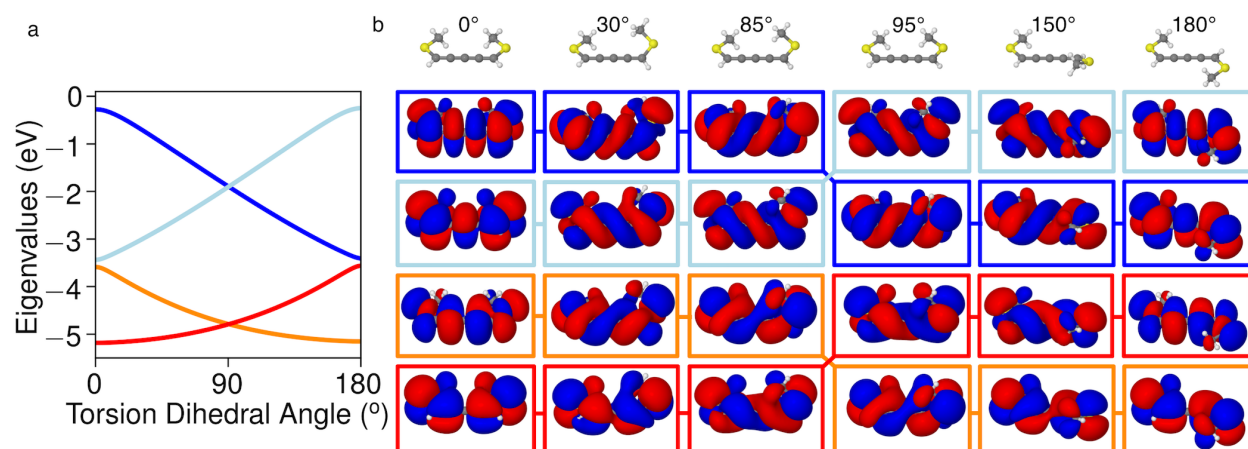systems are separated by symmetry because the end-groups are co-planar, and finally take the normal rectilinear shape.

Figure 8. Change of the frontier molecular orbitals of **[4]cumulene-SMe** under axial torsion. a) Eigenvalues of the frontier molecular orbitals plotted as a function of dihedral angle. b) Iso-plot of the four frontier molecular orbitals at dihedrals angles of 0°, 30°, 85°, 95°, 150°, and 180°, the molecular structures are shown at the top, followed by the LUMO+1, LUMO, HOMO, and HOMO–1 at the bottom.

ELECTRON TRANSPORT. Shown in Figure 9, the ballistic current density and electronic transmission is calculated for **[4]cumulene-SMe** under axial torsion. Strong ring currents are present around the wire near the ground-state structure with perpendicular end-groups (current density arrows are blue or red due to the large θ vector-component, see also Figure S26 and S27). Depending on the direction of torsion from 90° the ring currents have opposite directions, again in direct correlation with the change of orbital helicity at 90° (see Figure 8). Consequently, the ring currents are counter-clockwise around the wire at 85° torsion angle and clockwise around the wire at 95° torsion angle (arrows are red/blue due to positive/negative θ vector component). Different from **[5]cumulene-SMe** and **triyne-SMe** where the ring currents are centered around bonds, the

ring currents of **[4]cumulene-SMe** are centered around the atoms. The ring currents around the wire persist even as the torsion angles approach 0°/180° . With co-planar end-groups the direction of the ring current alternates with the ring currents centered around the wire are centered around the bonds rather than the atoms; these ring current remain although there is no clear helicity in the frontier orbitals of these configurations of the molecule (see Figure 8). By inspection, the current density appears more turbulent in the co-planar configurations, see Figure S25-S28 in Supporting Information.

From the transmissions plotted in Figure 9b, it is clear that the transmission at all torsion angles is dominated by a sharp antiresonance near the Fermi energy. Despite breaking the near-degeneracy of the frontier orbitals at 90° torsion, this suppression of the transmission remains within the HOMO-LUMO gap. The energy of the antiresonance is subject to the Fermi energy alignment which cannot reliably be determined using density functional theory (DFT); we return to this issue in the discussion section. As we use s-band electrodes in the calculations presented here, the Fermi energy is almost unchanged with torsion. Therefore we see in Figure 9b that as the HOMO-LUMO gap narrows when the torsion angle approaches 0°/180°, the transmission at the Fermi energy rises. As seen in other π-conjugated molecules, strong ring currents often appear when there are antiresonances in the transmission.[57] However, the total current is also very low in such cases as the transmission is suppressed. It is visually clear that the circular currents are stronger than the net current through the molecules. As the torsion angles approach 0°/180° the total current becomes higher and the current density pattern alternates in terms of its circular direction.

The transmission profile of even-*n* cumulenes under torsion is different from both polyynes and odd-*n* cumulenes. This clearly reveals the need to consider even-*n* and odd-*n* cumulenes as separate

classes of carbon wires until the true polymeric limit of carbyne is reached. Shown in Figure 9c

for **[4]cumulene-SMe** under axial torsion from the ground-state structure at 90°, the transmission

at the Fermi energy initially has a dihedral angle dependence similar to that of polyynes and

biphenyls. However, as the molecule approach a structure with co-planar end-groups the HOMO-

LUMO gap narrows and the transmission becomes higher than in polyynes and odd-n cumulenes

with equivalent torsion angles. The high transmission of even-n cumulenes in the co-planar

(unstable) configuration is likely what has been interpreted as an odd-even effect in previous

studies.[3-5, 72-84] However, such a trend depends on the choice of structure and is not a general

property of the cumulenic or polyynic nature of the molecule.

Unlike **triyne-SMe** and **[5]cumulene-SMe** which we examined in the previous two sections,

the trend shown in Figure 9c for **[5]cumulene-SMe** is subject to the Fermi energy alignment due

to the antiresonance in the transmission. However, we shall see in the next section that the

predicted trend in the transmission is a general feature of even-n cumulenic wires.
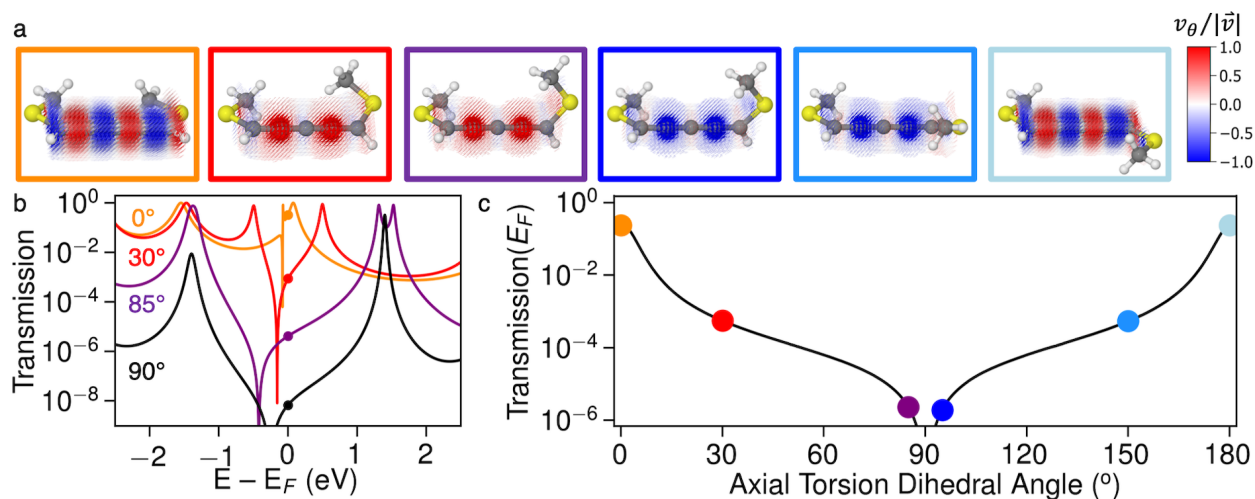

Figure 9. Current density and transmission of **[4]cumulene-SMe** under axial torsion. A) Current

density calculated at the Fermi energy colored by the normalized θ vector component at dihedral

angles (from left to right) 0°, 30°, 85°, 95°, 150°, and 180°. The current density vector field is

plotted as arrows that are normalized in each plot; each arrow is colored by its circular vector component (v_θ) normalized relative to its total vector length. High resolution images are included in SI part H, and scripts for generating 3D rotatable models are available online. b) Transmission plotted semilogarithmically against energy at select dihedral angles. c) Transmission at the fermi energy plotted against the torsion dihedral angle.

DISCUSSION

In the three results sections we have shown that three distinct transmission profiles exist for **triyne-SMe**, **[5]cumulene-SMe**, and **[4]cumulene-SMe**. We expect these trends to be largely independent of functional groups as all closed-shell carbon wires are expected to fall within the three types of linear carbon wires (in the limit that they can be considered molecules); two examples are included in SI part C.

In our computational studies of **triyne-SMe**, **[5]cumulene-SMe**, and **[4]cumulene-SMe** we strictly deal with the singlet ground-state as determined using DFT. It is clear that this approach may not be sufficient in systems with high diradical character,[110] such as **[5]cumulene-SMe** in configurations approaching 90° and **[4]cumulene-SMe** approaching 0°. Tests using complete active space self-consistent field (CASSCF) presented in SI part A suggest the discrepancy may be qualitative, although we are not able to verify this with transport calculations at the same level of theory. In potential transport experiments where a substantial bias is applied, the diradical character is likely to become zwitterionic character due to the electric field.[20] Further work must be done to fully understand such cases where the ground-state HOMO-LUMO gap vanishes.

The increasing open-shell character of **[5]cumulene-SMe** provides a compelling explanation for its rising transmission with torsion towards 90°. The increasing open-shell character can be

assessed in an intuitive way by drawing the dominant resonant structures of the molecules.[55, 67, 111] Shown in Scheme 1, at 0° torsion both **[5]cumulene-SMe** and **triyne-SMe** have a dominant closed-shell resonance structure and consequently both molecules have a significant HOMO-LUMO gap. However, at 90° torsion **[5]cumulene-SMe** only has diradical resonance structures and thus its HOMO-LUMO gap vanishes. As the HOMO-LUMO gap gradually becomes smaller with torsion towards 90°, the diradical character of the molecule rises as evident from the CASSCF calculation in Figure S1. As suggested by Stuyver et al.,[111] increase in diradical character is intimately related with high transmission. **Triyne-SMe** is still able to retain its closed-shell electron structure at 90°, and therefore has no effect like this. Although [4]cumulene-SMe has closed-shell electron structure at 90°, its rising transmission towards 0° torsion cannot be explained by drawing a single dominant resonance structure. Still, the HOMO-LUMO gap almost vanishes at 0°, and consequently the molecule has notable diradical character and high transmission (cf. Figure S1).

Scheme 1: Dominant resonance structures change with torsion.
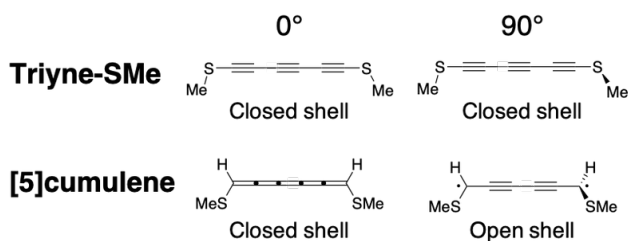
LENGTH DEPENDENCE. The wires we examined here are short molecules. It is clear that the trends will break down at some length. When the polymeric limit of true carbyne is reached, its properties will be those of the polyynic or the cumulenic structure because the odd-n and even-n of cumulenes is an edge effect. Furthermore, coherent off-resonant transport is not likely to be the dominant charge transport mechanism in very long molecular wires where structural fluctuations

and distortions may change the effect of torsion. From a purely theoretical perspective, we expect the trends to be qualitatively independent of molecular length because all three types of wires are isolobal with alternant molecular systems,[39, 114-115] and the change of the electronic structure with length is systematic in finite molecular systems.[70, 116] To a certain extent this can be verified with calculations on finite-length molecules. In Figure 10, we show the transmission profile under axial torsion for the three types of linear carbon wires with lengths of 21, 22, 31, and 32 atoms. The plots are very similar to those for the short wires we explored in the previous sections, and barely change when going from 22 (21) to 32 (31) atoms in the wire. At the scale of length where these transmission profiles may change coherent off-resonant transport is unlikely to be effective. Within the limit of coherent transport, axial torsion may serve as a test for whether a wire is in the molecular regime with three different structure types, or if the wire has reached the polymeric limit of carbyne where there are only two structure types.
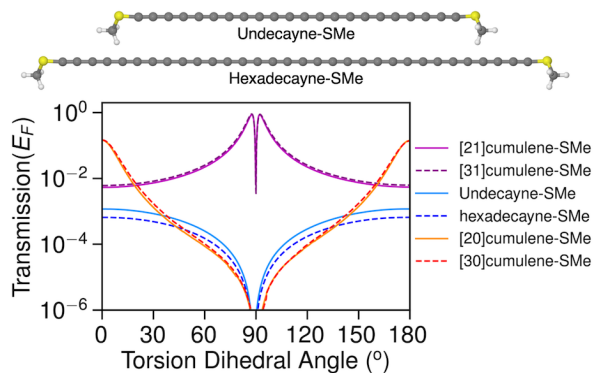
Figure 10. Top) Optimized molecular structures of thiomethyl-functionalized **undecayne-SMe** (22 carbon polyyne) and **hexadecayne-SMe** (32 carbon polyyne). Bottom) Transmission at the Fermi energy plotted against the axial torsion dihedral angle for long thiomethyl-functionalized cumulenic and polyyynic molecular wires.

JUNCTION MODELS. In the three results sections we calculated the transmission with wide-band approximated s-band electrodes using DFT. This approach has the advantage of not being

electrode-specific (what we calculate are properties of the molecule) and the electronic structure is calculated at a reasonable level of theory. Still, we think it is worthwhile to consider the generality of our approach. In Figure 11, we have furthermore carried out the transmission calculations using Hückel theory with s-band electrodes and DFT with Au-electrodes (we refer to the method section for computational details), the full transmission plots are included in SI part D. The transmission profiles with torsion are very similar with these three types of calculations. Using Hückel theory the electronic structure is idealized, and consequently perfect suppression is achieved at exactly 90° in all systems. Using DFT with Au-electrodes electronic degeneracies are broken and full suppression is never achieved; bulky Au electrodes may furthermore have higher coupling into the σ-systems of the molecules. It is clear that the trend of the transmission with axial torsion is very consistent from the most simplified level of theory to DFT calculations where the metal electrodes are fully considered. These trends are to be observed in single-molecule junction experiments if suitable ways of controlling the axial torsion can be realized, for example by constrained molecular designs or rotatable electrodes.
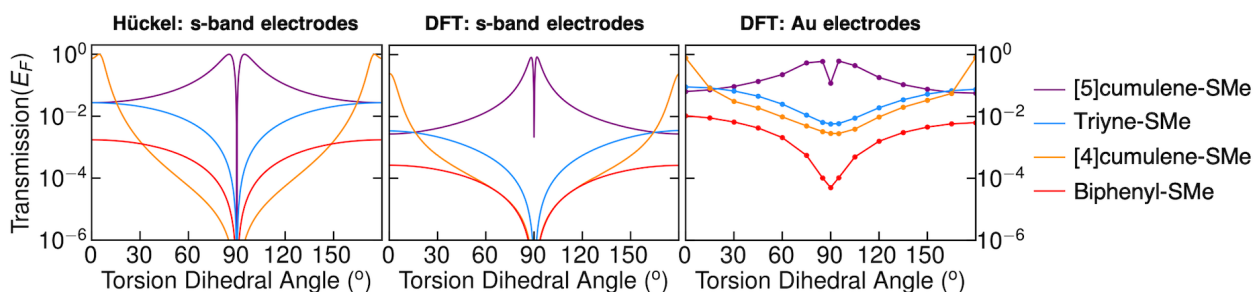

Figure 11. Transmission at the Fermi energy plotted against the axial torsion dihedral angle using three different calculation setups. Left) Using a simple Hückel model. Note that for [4]cumulene $E_F = -0.1$ eV. Middle) Using DFT with wide-band approximated s-band electrodes. Right) Using DFT with periodic Au electrodes.

We note that the Hückel calculations (SI part F) provide further insight into the suppression of the transmission in even-n cumulenes due to destructive quantum interference. At this level of theory, the antiresonance in the transmission of **[4]cumulene-SMe** is exactly in the middle of the HOMO-LUMO gap (the Fermi energy), and while the HOMO-LUMO gap narrows as the torsion angles approaches 0°/180° the antiresonance does not change energy (see Figure S7). Therefore, we plot the transmission at E_F = -0.1 eV for **[4]cumulene-SMe** in Figure 11. However, this also shows that the antiresonance is not affected by the torsion and given it is unusual that the antiresonance is exactly at the Fermi energy in a realistic setup, we find that the trends presented in Figure 11 are more likely to be observed in an actual experiment.

DEGENERATE ORBITALS AND DESTRUCTIVE INTERFERENCE. It is evident from the results, and specifically from Figure 11, that all three types of carbon chains experience a steep drop in the transmission at 90°. In all three cases this coincides with π-orbitals crossing each other, i.e., two molecular orbitals of opposite helicity become quasi-degenerate (see Figures 4, 6, and 8). As described in previous work by us and others,[45, 117] this can be understood as destructive quantum interference due opposite phase-symmetry of the near-degenerate orbital pairs. This symmetry rule follows directly from the analysis of the zeroth-order Green's functions pioneered by Yoshizawa and co-workers, an analysis which is exact at the Hückel level of theory and is general for all π-systems.[115, 117-118] Within this approximate description, the transmission is proportional to the square of the sum of contributions from each molecular orbital with index i, as written in equation 5.

$$T(E) \propto \left(\sum_i \frac{c_{i,L} \cdot c_{i,R}}{\epsilon_i - E} \right)^2 \qquad (5)$$

Here, $c_{i,L}$ and $c_{i,R}$ are the coefficients (weight and phase) of the i'th molecular orbital on the left L) and right (R) points of injection (the sulfur atoms), ε_i is the eigenvalue, and E is the injection

energy variable. Now assume the specific case where two frontier molecular orbitals, e.g. the HOMO and HOMO–1, become degenerate and have same absolute value of coefficients on the left and right side. This is exemplified in equation 6 with $T_{HOMO/HOMO-1}$ being the contribution from the HOMO and HOMO–1 to the complete sum in equation 5.

$$T_{HOMO/HOMO-1}(E) \propto (c_{HOMO,L} \cdot c_{HOMO,R} + c_{HOMO-1,L} \cdot c_{HOMO-1,R})^2 \qquad (6)$$

If the degenerate pair of molecular orbitals have the opposite sign in $c_{i,L/R}$ of each other on exactly one of the two terminal sites, then the orbital pair will not contribute to the total transmission.

Let us examine the phases (the sign of $c_{i,L/R}$) at the sulfur atoms of the frontier molecular orbital pairs at 90° (cf. Figure 4, 6, and 8). Shown in Figure 12, we choose a frontier orbital pair for each of the three molecular systems and assess the the sign of $c_{i,L/R}$. The phase is determined in an approximate way by observing the orientation of the π-orbitals on the sulfur, that is, which direction the blue/red lobes are pointing. We plot this as a Newman projection in the rightmost column to provide a simple tool of assessment of $c_{i,L/R}$. In **triyne-SMe** the HOMO and HOMO–1 are quasi-degenerate, and while the phases are the same for the horizontal lobes ($c_{i,R}$), it differs for the vertical lobes ($c_{i,L}$). Consequently, the contribution to the total transmission from the HOMO and HOMO–1 cancels out. In **[5]cumulene-SMe**, it is the HOMO and LUMO that are quasi-degenerate at 90° torsion. While the phases here are the same for the vertical lobes ($c_{i,L}$), they are opposite for the horizontal lobes ($c_{i,R}$). Likewise, in **[4]cumulene-SMe** the HOMO and HOMO–1 are quasi-degenerate and have opposite phase only for the vertical lobes. For all three systems, we can understand that the contributions to the transmission from the helical π-orbitals must cancel each other out whenever orbitals of opposite helicity become quasi-degenerate. This is in close analogy to similar systems where such cases of destructive quantum interference has been

described in detail.[45, 117, 119-121] Though we only assess one pair of frontier orbitals for each molecule here, other pairs of helical π-orbitals also become degenerate at 90°, in accordance with the Coulson-Rushbrooke orbital pairing theorem.[39, 114-115] We conclude from this analysis, that even though helical π-orbitals only have pseudo π-symmetry given the nodal planes follow a helix, the same theoretical analysis of destructive quantum interference applies as in the general case for π-systems.
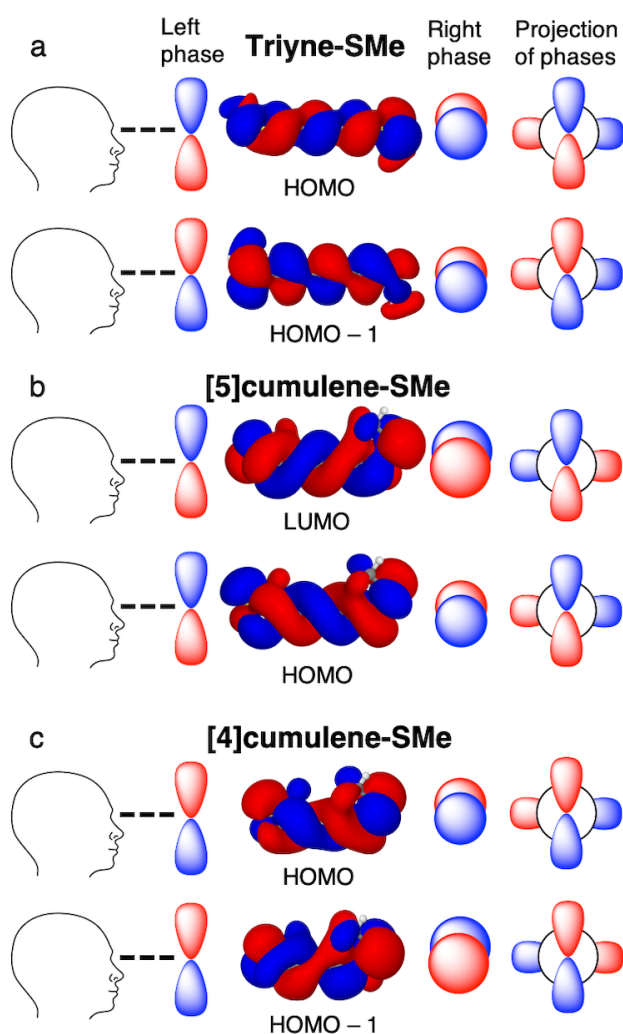

Figure 12. Overview of the relative phases of quasi-degenerate molecular orbitals at the terminal sites of **triyne-SMe** (a), **[5]cumulene-SMe** (b), and **[4]cumulene-SMe** (c), at 90° torsion angle.

Note, that it is different which molecular orbitals become quasi-degenerate for each system, cf. Figure 4, 6, and 8. This assessment is qualitative because the phases at the left and right termini are determined at arbitrary points, and the Newman projection (right column) should only be considered as a diagram.

CONCLUSIONS

In this work we have traced the change of electronic structure, ballistic current density, and Landauer transmission of linear carbon wires during axial torsion. All types of cumulenic and polyynic carbon wires exhibit helical π-orbitals when the end-groups are not in co-planar orientation. This helical electronic structure gives rise to ring current patterns around the linear wires, and for all three classes of wires we see a correlation between the change of frontier orbital helicities and the direction of the ring currents around the wire. It is hard not to speculate that ring current patterns around the axis of linear molecular wires can provide novel functionality in carbyne-based molecular electronics components. For example, it has been suggested that helical currents around an axis can induce a unidirectional rotation in the molecule due to the conservation of the total angular momentum,[122-123] thus making the linear segment of the molecule function as a current-driven motor. The circular movement of charge will also generate a local unidirectional magnetic field in the molecule,[124-125] which may allow for magnetic control of the single-molecule conductance;[126-130] a direction we are working towards exploring. Realizing the potential of helical currents in truly linear molecules poses an interesting challenge for the field of molecular electronics.

We have demonstrated that polyynes, odd-n cumulenes, and even-n cumulenes exhibit distinctively different transmission profiles under axial torsion. Most notably, we predict that the

transmission of odd-*n* cumulenes rise with torsion from 0°/180° towards 90° dihedral angle. The rise of transmission with torsion towards perpendicular end-groups is mediated by a narrowing of the HOMO-LUMO gap. This effect is also seen in even-*n* cumulenes when they approach a structure with co-planar end-groups. However, the electronic structure of polyynes do not provide any significant narrowing of the HOMO-LUMO gap with torsion, where the transmission follows the well-known cosine-squared dependence of the transmission with axial torsion. It is clear from our results, that the cosine-squared dependence is a special case which for linear carbon wires only holds for even-carbon polyynic systems. Common for all three types of carbon wires is that the transmission through the π-system is suppressed at 90° torsion. This is a direct consequence of molecular orbitals of opposite symmetry becoming quasi-degenerate, which leads to destructive quantum interference similar to that seen in cyclic π-systems.

The finding of three distinctive transmission profiles with torsion suggest that odd-*n* and even-*n* cumulenes are to be considered as separate types of carbyne-like molecules. Along with polyynes, odd-*n* and even-*n* cumulenes form the three classes of closed-shell carbon wires in the molecular limit. The identification of three regimes of axial torsion may allow for the identification of the polyynic or cumulenic nature of experimentally accessible carbyne wires.

Supporting Information. Level of Theory. Electronic Structure of Biphenyl. Alternative End-groups. Transmission Plots. Transmission with Gold Electrodes. Hückel Models. Convergence of Current Density. High Resolution Images of Current Density.

AUTHOR INFORMATION

Corresponding Author

*gsolomon@chem.ku.dk

Present Addresses

†Marc H. Garner: Laboratory for Computational Molecular Design, Institute of Chemical

Sciences and Engineering, École Polytechnique Fedérale de Lausanne, CH-1015 Lausanne,

Switzerland

REFERENCES

1.   Casari, C. S.; Milani, A. Carbyne: From the Elusive Allotrope to Stable Carbon Atom
Wires. *MRS Commun.* **2018**, *8*, 207-219.
2.   Banhart, F. Chains of Carbon Atoms: A Vision or a New Nanomaterial? *Beilstein J.
Nanotechnol.* **2015**, *6*, 559-569.
3.   Lang, N. D.; Avouris, P. Oscillatory Conductance of Carbon-Atom Wires. *Phys. Rev.
Lett.* **1998**, *81*, 3515-3518.
4.   Lang, N. D.; Avouris, P. Carbon-Atom Wires: Charge-Transfer Doping, Voltage Drop,
and the Effect of Distortions. *Phys. Rev. Lett.* **2000**, *84*, 358-361.
5.   Tongay, S.; Senger, R. T.; Dag, S.; Ciraci, S. Ab-Initio Electron Transport Calculations
of Carbon Based String Structures. *Phys. Rev. Lett.* **2004**, *93*, 136404.
6.   Artyukhov, V. I.; Liu, M.; Yakobson, B. I. Mechanically Induced Metal–Insulator
Transition in Carbyne. *Nano Lett.* **2014**, *14*, 4224-4229.
7.   La Torre, A.; Botello-Mendez, A.; Baaziz, W.; Charlier, J. C.; Banhart, F. Strain-Induced
Metal–Semiconductor Transition Observed in Atomic Carbon Chains. *Nat. Commun.* **2015**, *6*,
6636.
8.   Milani, A.; Tommasini, M.; Barbieri, V.; Lucotti, A.; Russo, V.; Cataldo, F.; Casari, C. S.
Semiconductor-to-Metal Transition in Carbon-Atom Wires Driven by Sp2 Conjugated End
Groups. *J. Phys. Chem. C* **2017**, *121*, 10562-10570.
9.   Lagow, R. J.; Kampa, J. J.; Wei, H.-C.; Battle, S. L.; Genge, J. W.; Laude, D. A.; Harper,
C. J.; Bau, R.; Stevens, R. C.; Haw, J. F., et al. Synthesis of Linear Acetylenic Carbon: The
Carbon Allotrope. *Science* **1995**, *267*, 362.

10.   Szafert, S.; Gladysz, J. A. Carbon in One Dimension: Structural Analysis of the Higher Conjugated Polyynes. *Chem. Rev.* **2003**, *103*, 4175-4206.

11.   Chalifoux, W. A.; Tykwinski, R. R. Synthesis of Polyynes to Model the Sp-Carbon Allotrope Carbyne. *Nat. Chem.* **2010**, *2*, 967-971.

12.   Casari, C. S.; Tommasini, M.; Tykwinski, R. R.; Milani, A. Carbon-Atom Wires: 1-D Systems with Tunable Properties. *Nanoscale* **2016**, *8*, 4414-4435.

13.   Wendinger, D.; Tykwinski, R. R. Odd [N]Cumulenes (N = 3, 5, 7, 9): Synthesis, Characterization, and Reactivity. *Acc. Chem. Res.* **2017**, *50*, 1468-1479.

14.   Wang, C.; Batsanov, A. S.; Bryce, M. R.; Martín, S.; Nichols, R. J.; Higgins, S. J.; García-Suárez, V. M.; Lambert, C. J. Oligoyne Single Molecule Wires. *J. Am. Chem. Soc.* **2009**, *131*, 15647-15654.

15.   Ballmann, S.; Hieringer, W.; Secker, D.; Zheng, Q.; Gladysz, J. A.; Görling, A.; Weber, H. B. Molecular Wires in Single-Molecule Junctions: Charge Transport and Vibrational Excitations. *ChemPhysChem* **2010**, *11*, 2256-2260.

16.   Milan, D. C.; Al-Owaedi, O. A.; Oerthel, M.-C.; Marqués-González, S.; Brooke, R. J.; Bryce, M. R.; Cea, P.; Ferrer, J.; Higgins, S. J.; Lambert, C. J., et al. Solvent Dependence of the Single Molecule Conductance of Oligoyne-Based Molecular Wires. *J. Phys. Chem. C* **2016**, *120*, 15666-15674.

17.   Milan, D. C.; Krempe, M.; Ismael, A. K.; Movsisyan, L. D.; Franz, M.; Grace, I.; Brooke, R. J.; Schwarzacher, W.; Higgins, S. J.; Anderson, H. L., et al. The Single-Molecule Electrical Conductance of a Rotaxane-Hexayne Supramolecular Assembly. *Nanoscale* **2017**, *9*, 355-361.

18.   Jasper-Tönnies, T.; Garcia-Lekue, A.; Frederiksen, T.; Ulrich, S.; Herges, R.; Berndt, R. Conductance of a Freestanding Conjugated Molecular Wire. *Phys. Rev. Lett.* **2017**, *119*, 066801.

19.   Xu, W.; Leary, E.; Hou, S.; Sangtarash, S.; González, M. T.; Rubio-Bollinger, G.; Wu, Q.; Sadeghi, H.; Tejerina, L.; Christensen, K. E., et al. Unusual Length Dependence of the Conductance in Cumulene Molecular Wires. *Angew. Chem. Int. Ed.* **2019**, *58*, 8378-8382.

20.   Zang, Y.; Zou, Q.; Fu, T.; Ng, F.; Fowler, B.; Yang, J.; Li, H.; Steigerwald, M. L.; Nuckolls, C.; Venkataraman, L. Directing Isomerization Reactions of Cumulenes with Electric Fields. *Nat. Commun.* **2019**, *10*, 4482.

21.   Yuzvinsky, T. D.; Mickelson, W.; Aloni, S.; Begtrup, G. E.; Kis, A.; Zettl, A. Shrinking a Carbon Nanotube. *Nano Lett.* **2006**, *6*, 2718-2722.

22.   Ravagnan, L.; Piseri, P.; Bruzzi, M.; Miglio, S.; Bongiorno, G.; Baserga, A.; Casari, C. S.; Li Bassi, A.; Lenardi, C.; Yamaguchi, Y., et al. Influence of Cumulenic Chains on the Vibrational and Electronic Properties of Sp-Sp2 Amorphous Carbon. *Phys. Rev. Lett.* **2007**, *98*, 216103.

23.   Jin, C.; Lan, H.; Peng, L.; Suenaga, K.; Iijima, S. Deriving Carbon Atomic Chains from Graphene. *Phys. Rev. Lett.* **2009**, *102*, 205501.

24.   Börrnert, F.; Börrnert, C.; Gorantla, S.; Liu, X.; Bachmatiuk, A.; Joswig, J.-O.; Wagner, F. R.; Schäffel, F.; Warner, J. H.; Schönfelder, R., et al. Single-Wall-Carbon-Nanotube/Single-Carbon-Chain Molecular Junctions. *Phys. Rev. B* **2010**, *81*, 085439.

25.   Cretu, O.; Botello-Mendez, A. R.; Janowska, I.; Pham-Huu, C.; Charlier, J.-C.; Banhart, F. Electrical Transport Measured in Atomic Carbon Chains. *Nano Lett.* **2013**, *13*, 3487-3493.

26.   Shi, L.; Rohringer, P.; Suenaga, K.; Niimi, Y.; Kotakoski, J.; Meyer, J. C.; Peterlik, H.; Wanko, M.; Cahangirov, S.; Rubio, A., et al. Confined Linear Carbon Chains as a Route to Bulk Carbyne. *Nat. Mater.* **2016**, *15*, 634-639.

27.   Ben Romdhane, F.; Adjizian, J.-J.; Charlier, J.-C.; Banhart, F. Electrical Transport through Atomic Carbon Chains: The Role of Contacts. *Carbon* **2017**, *122*, 92-97.

28.   Woitellier, S.; Launay, J. P.; Joachim, C. The Possibility of Molecular Switching: Theoretical Study of [(Nh3)5ru-4,4′-Bipy-Ru(Nh3)5]5+. *Chem. Phys.* **1989**, *131*, 481-488.

29.   Mujica, V.; Nitzan, A.; Mao, Y.; Davis, W.; Kemp, M.; Roitberg, A.; Ratner, M. A. Electron Transfer in Molecules and Molecular Wires: Geometry Dependence, Coherent Transfer, and Control. *Advances in Chemical Physics* **1999**, *107*, 403-429.

30.   Venkataraman, L.; Klare, J. E.; Nuckolls, C.; Hybertsen, M. S.; Steigerwald, M. L. Dependence of Single-Molecule Junction Conductance on Molecular Conformation. *Nature* **2006**, *442*, 904-907.

31.   Vonlanthen, D.; Mishchenko, A.; Elbing, M.; Neuburger, M.; Wandlowski, T.; Mayor, M. Chemically Controlled Conductivity: Torsion-Angle Dependence in a Single-Molecule Biphenyldithiol Junction. *Angew. Chem. Int. Ed.* **2009**, *48*, 8886-8890.

32.   Mishchenko, A.; Vonlanthen, D.; Meded, V.; Bürkle, M.; Li, C.; Pobelov, I. V.; Bagrets, A.; Viljas, J. K.; Pauly, F.; Evers, F., et al. Influence of Conformation on Conductance of Biphenyl-Dithiol Single-Molecule Contacts. *Nano Lett.* **2010**, *10*, 156-163.

33.   Cui, L.; Liu, B.; Vonlanthen, D.; Mayor, M.; Fu, Y.; Li, J.-F.; Wandlowski, T. In Situ Gap-Mode Raman Spectroscopy on Single-Crystal Au(100) Electrodes: Tuning the Torsion Angle of 4,4′-Biphenyldithiols by an Electrochemical Gate Field. *J. Am. Chem. Soc.* **2011**, *133*, 7332-7335.

34.   Bürkle, M.; Viljas, J. K.; Vonlanthen, D.; Mishchenko, A.; Schön, G.; Mayor, M.; Wandlowski, T.; Pauly, F. Conduction Mechanisms in Biphenyl Dithiol Single-Molecule Junctions. *Phys. Rev. B* **2012**, *85*, 075417.

35.   Chen, Z.; Chen, L.; Liu, J.; Li, R.; Tang, C.; Hua, Y.; Chen, L.; Shi, J.; Yang, Y.; Liu, J., et al. Modularized Tuning of Charge Transport through Highly Twisted and Localized Single-Molecule Junctions. *J. Phys. Chem. Lett.* **2019**, *10*, 3453-3458.

36.   Fischer, H.; Kollmar, H. Zur Invarianz in Der Lcao Mo Theorie. *Theor. Chim. Acta* **1968**, *12*, 344-348.

37.   Zimmerman, H. E. Moebius-Hueckel Concept in Organic Chemistry. Application of Organic Molecules and Reactions. *Acc. Chem. Res.* **1971**, *4*, 272-280.

38.   Herges, R. Coarctate and Pseudocoarctate Reactions: Stereochemical Rules. *J. Org. Chem.* **2015**, *80*, 11869-11876.

39.   Garner, M. H.; Hoffmann, R.; Rettrup, S.; Solomon, G. C. Coarctate and Möbius: The Helical Orbitals of Allene and Other Cumulenes. *ACS Cent. Sci.* **2018**, *4*, 688-700.

40.   Hendon, C. H.; Tiana, D.; Murray, A. T.; Carbery, D. R.; Walsh, A. Helical Frontier Orbitals of Conjugated Linear Molecules. *Chem. Sci.* **2013**, *4*, 4278-4284.

41.   Tiana, D.; Hendon, C. H.; Walsh, A. Ligand Design for Long-Range Magnetic Order in Metal–Organic Frameworks. *Chem. Comm.* **2014**, *50*, 13990-13993.

42.   Liu, M.; Artyukhov, V. I.; Lee, H.; Xu, F.; Yakobson, B. I. Carbyne from First Principles: Chain of C Atoms, a Nanorod or a Nanorope. *ACS Nano* **2013**, *7*, 10075-10082.

43.   Imamura, A.; Aoki, Y. Helical Molecular Orbitals around Straight-Chain Polyyne Oligomers as Models for Molecular Devices. *Chem. Phys. Lett.* **2013**, *590*, 136-140.

44.   Peeks, M. D.; Neuhaus, P.; Anderson, H. L. Experimental and Computational Evaluation of the Barrier to Torsional Rotation in a Butadiyne-Linked Porphyrin Dimer. *Phys. Chem. Chem. Phys.* **2016**, *18*, 5264-5274.

45.   Garner, M. H.; Jensen, A.; Hyllested, L. O. H.; Solomon, G. C. Helical Orbitals and Circular Currents in Linear Carbon Wires. *Chem. Sci.* **2019**, *10*, 4598-4608.

46.   Garner, M. H.; Jensen, A.; Hyllested, L. O. H.; Solomon, G. C. Correction: Helical Orbitals and Circular Currents in Linear Carbon Wires. *Chem. Sci.* **2020**, *11*, 2568-2571.

47.   Orimoto, Y.; Aoki, Y.; Imamura, A. Extraction of One-Handed Helical Frontier Orbital in Even [N]Cumulenes by Breaking Mirror Images of Right- and Left-Handed Helical Orbitals: Theoretical Study. *J. Phys. Chem. C* **2019**, *123*, 11134-11139.

48.   Guo, Y.-D.; Yan, X.-H.; Xiao, Y. Conformational Change-Induced Switching Behavior in Pure-Carbon Systems. *RSC Adv.* **2013**, *3*, 16672-16680.

49.   Caricato, M. Orbital Analysis of Molecular Optical Activity Based on Configuration Rotatory Strength. *J. Chem. Theory Comput.* **2015**, *11*, 1349-1353.

50.   Sarbadhikary, P.; Shil, S.; Panda, A.; Misra, A. A Perspective on Designing Chiral Organic Magnetic Molecules with Unusual Behavior in Magnetic Exchange Coupling. *J. Org. Chem.* **2016**, *81*, 5623-5630.

51.   Gluyas, J. B. G.; Gückel, S.; Kaupp, M.; Low, P. J. Rational Control of Conformational Distributions and Mixed-Valence Characteristics in Diruthenium Complexes. *Chem. Eur. J.* **2016**, *22*, 16138-16146.

52.   Gückel, S.; Gluyas, J. B. G.; El-Tarhuni, S.; Sobolev, A. N.; Whiteley, M. W.; Halet, J.-F.; Lapinte, C.; Kaupp, M.; Low, P. J. Iron Versus Ruthenium: Clarifying the Electronic Differences between Prototypical Mixed-Valence Organometallic Butadiyndiyl Bridged Molecular Wires. *Organometallics* **2018**, *37*, 1432-1445.

53.   Martin, W. R.; Ball, D. W. Small Organic Azides as High Energy Materials: Perazidoacetylene, -Ethylene, and -Allene. *ChemistrySelect* **2018**, *3*, 7222-7225.

54.   Martin, W. R.; Ball, D. W. Small Organic Fulminates as High Energy Materials. Fulminates of Acetylene, Ethylene, and Allene. *J. Energ. Mater.* **2019**, *37*, 70-79.

55.   Garner, M. H.; Bro-Jørgensen, W.; Pedersen, P. D.; Solomon, G. C. Reverse Bond-Length Alternation in Cumulenes: Candidates for Increasing Electronic Transmission with Length. *J. Phys. Chem. C* **2018**, *122*, 26777–26789.

56.   Jensen, A.; Garner, M. H.; Solomon, G. C. When Current Does Not Follow Bonds: Current Density in Saturated Molecules. *J. Phys. Chem. C* **2019**, *123*, 12042-12051.

57.   Solomon, G. C.; Herrmann, C.; Hansen, T.; Mujica, V.; Ratner, M. A. Exploring Local Currents in Molecular Junctions. *Nat. Chem.* **2010**, *2*, 223.

58.   Rai, D.; Hod, O.; Nitzan, A. Circular Currents in Molecular Wires. *J. Phys. Chem. C* **2010**, *114*, 20583-20594.

59.   Wilhelm, J.; Walz, M.; Evers, F. Ab Initio Quantum Transport through Armchair Graphene Nanoribbons: Streamlines in the Current Density. *Phys. Rev. B* **2014**, *89*, 195406.

60.   Stuyver, T.; Blotwijk, N.; Fias, S.; Paul, G.; De Proft, F. Exploring Electrical Currents through Nanographenes: Visualization and Tuning of the through-Bond Transmission Paths. *ChemPhysChem* **2017**, *18*, 3012-3022.

61.   Fias, S.; Stuyver, T. Extension of the Source-Sink Potential Approach to Hartree-Fock and Density Functional Theory: A New Tool to Visualize the Ballistic Current through Molecules. *J. Chem. Phys.* **2017**, *147*, 184102.

62.   Rix, J. B.; Hedegård, P. Thermoelectric Driven Ring Currents in Single Molecules and Graphene Nanoribbons. *J. Phys. Chem. C* **2019**, *123*, 3817-3822.

63.   Hoffmann, R. Extended Hückel Theory—V: Cumulenes, Polyenes, Polyacetylenes and Cn. *Tetrahedron* **1966**, *22*, 521-538.

64.   Kuhn, R.; Schulz, B.; Jochims, J. C. Cis-Trans-Isomerism of 1,6-Diphenyl-1,6-Di-T-Butylhexapentaene. *Angew. Chem. Int. Ed.* **1966**, *5*, 420-420.

65.   Auffrant, A.; Jaun, B.; Jarowski Peter, D.; Houk Kendall, N.; Diederich, F. Peralkynylated Buta-1,2,3-Trienes: Exceptionally Low Rotational Barriers of Cumulenic C=C Bonds in the Range of Those of Peptide Cn Bonds. *Chem. Eur. J.* **2004**, *10*, 2906-2911.

66.   Jarowski, P. D.; Diederich, F.; Houk, K. N. Butatrienes as Extended Alkenes: Barriers to Internal Rotation and Substitution Effects on the Stabilities of the Ground States and Transition States. *J. Phys. Chem. A* **2006**, *110*, 7237-7246.

67.   Buehringer, M. U.; Padberg, K.; Phleps, M.; Maid, H.; Placht, C.; Neiss, C.; Ferguson, M.; Goerling, A.; Tykwinski, R. R. Double Bonds? Studies on the Barrier to Rotation About the Cumulenic C=C Bonds of Tetraaryl[N]Cumulenes (N = 3, 5, 7, 9). *Angew. Chem. Int. Ed.* **2018**, *57*, 8321-8325.

68.   Imamura, A.; Aoki, Y. Electronic Structures and Molecular Structures of Polyynes. *Int. J. Quantum Chem.* **2013**, *113*, 423-427.

69.   Al-Backri, A.; Zólyomi, V.; Lambert, C. J. Electronic Properties of Linear Carbon Chains: Resolving the Controversy. *J. Chem. Phys.* **2014**, *140*, 104306.

70.   Lambropoulos, K.; Simserides, C. Electronic Structure and Charge Transport Properties of Atomic Carbon Wires. *Phys. Chem. Chem. Phys.* **2017**, *19*, 26890-26897.

71.   Sarbadhikary, P.; Shil, S.; Misra, A. Magnetic and Transport Properties of Conjugated and Cumulated Molecules: The [Small Pi]-System Enlightens Part of the Story. *Phys. Chem. Chem. Phys.* **2018**, *20*, 9364-9375.

72.   Larade, B.; Taylor, J.; Mehrez, H.; Guo, H. Conductance, I-V Curves, and Negative Differential Resistance of Carbon Atomic Wires. *Phys. Rev. B* **2001**, *64*, 075420.

73.   Khoo, K. H.; Neaton, J. B.; Son, Y. W.; Cohen, M. L.; Louie, S. G. Negative Differential Resistance in Carbon Atomic Wire-Carbon Nanotube Junctions. *Nano Lett.* **2008**, *8*, 2900-2905.

74.   Prasongkit, J.; Grigoriev, A.; Wendin, G.; Ahuja, R. Cumulene Molecular Wire Conductance from First Principles. *Phys. Rev. B* **2010**, *81*, 115404.

75.   Shen, L.; Zeng, M.; Yang, S.-W.; Zhang, C.; Wang, X.; Feng, Y. Electron Transport Properties of Atomic Carbon Nanowires between Graphene Electrodes. *J. Am. Chem. Soc.* **2010**, *132*, 11481-11486.

76.   Zanolli, Z.; Onida, G.; Charlier, J. C. Quantum Spin Transport in Carbon Chains. *ACS Nano* **2010**, *4*, 5174-5180.

77.   Song, B.; Sanvito, S.; Fang, H. Anomalous I–V Curve for Mono-Atomic Carbon Chains. *New J. Phys.* **2010**, *12*, 103017.

78.   Fürst, J. A.; Brandbyge, M.; Jauho, A. P. Atomic Carbon Chains as Spin-Transmitters: An Ab Initio Transport Study. *EPL* **2010**, *91*, 37002.

79.   Qiu, M.; Liew, K. M. Odd–Even Effects of Electronic Transport in Carbon-Chain-Based Molecular Devices. *J. Phys. Chem. C* **2012**, *116*, 11709-11713.

80.   D'yachkov, P. N.; Zaluev, V. A.; Kocherga, E. Y.; Sadykov, N. R. Tight Binding Model of Quantum Conductance of Cumulenic and Polyynic Carbynes. *J. Phys. Chem. C* **2013**, *117*, 16306-16315.

81.   Zhang, Z.; Zhang, J.; Kwong, G.; Li, J.; Fan, Z.; Deng, X.; Tang, G. All-Carbon Sp-Sp2 Hybrid Structures: Geometrical Properties, Current Rectification, and Current Amplification. *Sci. Rep.* **2013**, *3*, 2575.

82.   Oeiras, R. Y.; Silva, E. Z. d. Bond Length and Electric Current Oscillation of Long Linear Carbon Chains: Density Functional Theory, Mpb Model, and Quantum Spin Transport Studies. *J. Chem. Phys.* **2014**, *140*, 134703.

83.   Yu, J.-X.; Hou, Z.-W.; Liu, X.-Y. Stability of Conductance Oscillations in Carbon Atomic Chains. *Chinese Phys. B* **2015**, *24*, 067307.

84.   Fan, Z. Q.; Zhang, Z. H.; Deng, X. Q.; Tang, G. P.; Yang, C. H.; Sun, L.; Zhu, H. L. Effect of Electrode Twisting on Electronic Transport Properties of Atomic Carbon Wires. *Carbon* **2016**, *98*, 179-186.

85.   Garner, M. H.; Koerstz, M.; Jensen, J. H.; Solomon, G. C. The Bicyclo[2.2.2]Octane Motif: A Class of Saturated Group 14 Quantum Interference Based Single-Molecule Insulators. *J. Phys. Chem. Lett.* **2018**, *9*, 6941-6947.

86.   Perdew, J. P.; Burke, K.; Ernzerhof, M. Generalized Gradient Approximation Made Simple. *Phys. Rev. Lett.* **1996**, *77*, 3865-3868.

87.   Frisch, M. J.; Trucks, G. W.; Schlegel, H. B.; G. E. Scuseria; Robb, M. A.; Cheeseman, J. R.; Scalmani, G.; Barone, V.; B. Mennucci; Petersson, G. A., et al. *Gaussian 09, Rev. D.01*, Gaussian, Inc., Wallingford CT, 2013.: 2013.

88.   Enkovaara, J.; Rostgaard, C.; Mortensen, J. J.; Chen, J.; Dułak, M.; Ferrighi, L.; Gavnholt, J.; Glinsvad, C.; Haikola, V.; Hansen, H. A., et al. Electronic Structure Calculations with Gpaw: A Real-Space Implementation of the Projector Augmented-Wave Method. *J. Phys. Condens. Matter* **2010**, *22*, 253202.

89.   Larsen, A. H.; Mortensen, J. J.; Blomqvist, J.; Castelli, I. E.; Christensen, R.; Dułak, M.; Friis, J.; Groves, M. N.; Hammer, B.; Hargus, C., et al. The Atomic Simulation Environment—a Python Library for Working with Atoms. *J. Phys.: Condens. Matter* **2017**, *29*, 273002.

90.   Larsen, A. H.; Vanin, M.; Mortensen, J. J.; Thygesen, K. S.; Jacobsen, K. W. Localized Atomic Basis Set in the Projector Augmented Wave Method. *Phys. Rev. B* **2009**, *80*, 195112.

91.   Zhao, Y.; Truhlar, D. G. The M06 Suite of Density Functionals for Main Group Thermochemistry, Thermochemical Kinetics, Noncovalent Interactions, Excited States, and Transition Elements: Two New Functionals and Systematic Testing of Four M06-Class Functionals and 12 Other Functionals. *Theor. Chem. Acc.* **2008**, *120*, 215-241.

92.   Grimme, S.; Antony, J.; Ehrlich, S.; Krieg, H. A Consistent and Accurate Ab Initio Parametrization of Density Functional Dispersion Correction (Dft-D) for the 94 Elements H-Pu. *J. Chem. Phys.* **2010**, *132*, 154104.

93.   Aidas, K.; Angeli, C.; Bak, K. L.; Bakken, V.; Bast, R.; Boman, L.; Christiansen, O.; Cimiraglia, R.; Coriani, S.; Dahle, P., et al. The Dalton Quantum Chemistry Program System. *WIREs Comput. Mol. Sci.* **2014**, *4*, 269-284.

94.   Jmol: An Open-Source Java Viewer for Chemical Structures in 3d. http://www.jmol.org/.

95.   Datta, S., *Electronic Transport in Mesoscopic Systems*; Cambridge University Press, 1995.

96.   Xue, Y.; Ratner, M. A. Local Field Effects in Current Transport through Molecular Electronic Devices: Current Density Profiles and Local Nonequilibrium Electron Distributions. *Phys. Rev. B* **2004**, *70*, 081404.

97.   Zhang, L.; Wang, B.; Wang, J. First-Principles Calculation of Current Density in Molecular Devices. *Phys. Rev. B* **2011**, *84*, 115412.

98.   Cabra, G.; Jensen, A.; Galperin, M. On Simulation of Local Fluxes in Molecular Junctions. *J. Chem. Phys.* **2018**, *148*, 204103.

99.   Pohl, V.; Marsoner Steinkasserer, L. E.; Tremblay, J. C. Imaging Time-Dependent Electronic Currents through a Graphene-Based Nanojunction. *J. Phys. Chem. Lett.* **2019**, 5387-5394.

100.   Lai, L. Q.; Chen, J.; Liu, Q. H.; Yu, Y. B. Charge Nonconservation of Molecular Devices in the Presence of a Nonlocal Potential. *Phys. Rev. B* **2019**, *100*, 125437.

101.   Mayerle, J. J.; Flandera, M. A. Bis(1-Carbazolyl)Butadiyne. *Acta Cryst. B* **1978**, *34*, 1374-1376.

102.   Tokutome, Y.; Okuno, T. Preparations, Crystal Polymorphs and Dft Calculations of N1,N1,N4,N4-Tetraphenylbuta-1,3-Diyne-1,4-Diamine. *J. Mol. Struct.* **2013**, *1047*, 136-142.

103.   Cook, A. M.; Wolf, C. Terminal Ynamides: Synthesis, Coupling Reactions, and Additions to Common Electrophiles. *Tetrahedron Lett.* **2015**, *56*, 2377-2392.

104.   Doan, T.-H.; Talbi, I.; Lohier, J.-F.; Touil, S.; Alayrac, C.; Witulski, B. Synthesis, Crystal Structure, Optical, Electrochemical and Thermal Properties of the Ynamide: Bis-(N-4-Methylbenzenesulfonyl, N-N-Butyl)-1,3-Butadiyne-1,4-Diamide. *J. Mol. Struct.* **2016**, *1116*, 127-134.

105.   Pigulski, B.; Męcik, P.; Cichos, J.; Szafert, S. Use of Stable Amine-Capped Polyynes in the Regioselective Synthesis of Push–Pull Thiophenes. *J. Org. Chem.* **2017**, *82*, 1487-1498.

106.   Ravagnan, L.; Manini, N.; Cinquanta, E.; Onida, G.; Sangalli, D.; Motta, C.; Devetta, M.; Bordoni, A.; Piseri, P.; Milani, P. Effect of Axial Torsion on Sp Carbon Atomic Wires. *Phys. Rev. Lett.* **2009**, *102*, 245502.

107.   Petreska, I.; Pejov, L.; Kocarev, L. Controlling the Torsional Stochastic Switching in Phenylene Ethynylene Oligomer Molecules by External Electrostatic Fields. *Phys. Rev. B* **2008**, *78*, 045209.

108.   Dou, K. P.; De Sarkar, A.; Wang, C. L.; Zhang, R. Q. Intramolecular Torsion Based Molecular Switch Functionality Enhanced in Π-Conjugated Oligomolecules by a Π-Conjugated Pendant Group. *J. Phys. Chem. C* **2011**, *115*, 13911-13918.

109.   González, M. T.; Zhao, X.; Manrique, D. Z.; Miguel, D.; Leary, E.; Gulcur, M.; Batsanov, A. S.; Rubio-Bollinger, G.; Lambert, C. J.; Bryce, M. R., et al. Structural Versus Electrical Functionalization of Oligo(Phenylene Ethynylene) Diamine Molecular Junctions. *J. Phys. Chem. C* **2014**, *118*, 21655-21662.

110.   Gil-Guerrero, S.; Peña-Gallego, Á.; Ramos-Berdullas, N.; Martín Pendás, Á.; Mandado, M. Assessing the Reversed Exponential Decay of the Electrical Conductance in Molecular Wires: The Undeniable Effect of Static Electron Correlation. *Nano Lett.* **2019**, *19*, 7394-7399.

111.   Stuyver, T.; Zeng, T.; Tsuji, Y.; Geerlings, P.; De Proft, F. Diradical Character as a Guiding Principle for the Insightful Design of Molecular Nanowires with an Increasing Conductance with Length. *Nano Lett.* **2018**, *18*, 7298-7304.

112.   Kuang, G.; Chen, S.-Z.; Wang, W.; Lin, T.; Chen, K.; Shang, X.; Liu, P. N.; Lin, N. Resonant Charge Transport in Conjugated Molecular Wires Beyond 10 Nm Range. *J. Am. Chem. Soc.* **2016**, *138*, 11140-11143.

113.   Zang, Y.; Ray, S.; Fung, E. D.; Borges, A.; Garner, M. H.; Steigerwald, M. L.; Solomon, G. C.; Patil, S.; Venkataraman, L. Resonant Transport in Single Diketopyrrolopyrrole Junctions. *J. Am. Chem. Soc.* **2018**, *140*, 13167-13170.

114.   Coulson, C. A.; Rushbrooke, G. S. Note on the Method of Molecular Orbitals. *Math. Proc. Camb. Philos. Soc.* **1940**, *36*, 193-200.

115.   Zhao, X.; Geskin, V.; Stadler, R. Destructive Quantum Interference in Electron Transport: A Reconciliation of the Molecular Orbital and the Atomic Orbital Perspective. *J. Chem. Phys.* **2016**, *146*, 092308.

116.   Hoffmann, R. How Chemistry and Physics Meet in the Solid State. *Angew. Chem. Int. Ed.* **1987**, *26*, 846-878.

117.   Yoshizawa, K.; Tada, T.; Staykov, A. Orbital Views of the Electron Transport in Molecular Devices. *J. Am. Chem. Soc.* **2008**, *130*, 9406-9413.

118.   Tada, T.; Yoshizawa, K. Quantum Transport Effects in Nanosized Graphite Sheets. *ChemPhysChem* **2002**, *3*, 1035-1037.

119.   Sowa, J. K.; Mol, J. A.; Briggs, G. A. D.; Gauger, E. M. Spiro-Conjugated Molecular Junctions: Between Jahn–Teller Distortion and Destructive Quantum Interference. *J. Phys. Chem. Lett.* **2018**, *9*, 1859-1865.

120.   Härtle, R.; Butzin, M.; Rubio-Pons, O.; Thoss, M. Quantum Interference and Decoherence in Single-Molecule Junctions: How Vibrations Induce Electrical Current. *Phys. Rev. Lett.* **2011**, *107*, 046802.

121.   Ballmann, S.; Härtle, R.; Coto, P. B.; Elbing, M.; Mayor, M.; Bryce, M. R.; Thoss, M.; Weber, H. B. Experimental Evidence for Quantum Interference and Vibrationally Induced Decoherence in Single-Molecule Junctions. *Phys. Rev. Lett.* **2012**, *109*, 056801.

122.   Král, P.; Seideman, T. Current-Induced Rotation of Helical Molecular Wires. *J. Chem. Phys.* **2005**, *123*, 184702.

123.   Bailey, S. W. D.; Amanatidis, I.; Lambert, C. J. Carbon Nanotube Electron Windmills: A Novel Design for Nanomotors. *Phys. Rev. Lett.* **2008**, *100*, 256802.

124.   Walz, M.; Wilhelm, J.; Evers, F. Current Patterns and Orbital Magnetism in Mesoscopic Dc Transport. *Phys. Rev. Lett.* **2014**, *113*, 136602.

125.   Nozaki, D.; Schmidt, W. G. Current Density Analysis of Electron Transport through Molecular Wires in Open Quantum Systems. *J. Comp. Chem.* **2017**, *38*, 1685-1692.

126.   Hod, O.; Baer, R.; Rabani, E. A Parallel Electromagnetic Molecular Logic Gate. *J. Am. Chem. Soc.* **2005**, *127*, 1648-1649.

127.   Hod, O.; Rabani, E.; Baer, R. Magnetoresistance of Nanoscale Molecular Devices. *Acc. Chem. Res.* **2006**, *39*, 109-117.

128.   Rai, D.; Hod, O.; Nitzan, A. Magnetic Field Control of the Current through Molecular Ring Junctions. *J. Phys. Chem. Lett.* **2011**, *2*, 2118-2124.

129.   Rai, D.; Hod, O.; Nitzan, A. Magnetic Fields Effects on the Electronic Conduction Properties of Molecular Ring Structures. *Phys. Rev. B* **2012**, *85*, 155440.

130.   Dhakal, U.; Rai, D. Magnetic Field Control of Current through Model Graphene Nanosheets. *Phys. Lett. A* **2019**, *383*, 2193-2200.

TOC FIGURE

Polyyne?
Odd-*n* cumulene?
Even-*n* cumulene?